Precision mass measurement of ^{61}Zn and updated Ft value for conserved vector current tests

P. F. Giesel [1,*] D. Atanasov [2,†] K. Blaum [2] P. Fischer [1] J. Karthein [3,2] I. Kulikov [4] Yu. A. Litvinov [4,5] D. Lunney [6,‡,§] M. Mougeot [6,2,7] L. Nies [7,1] L. Schweikhard [1] V. A. Virtanen [8,9] and F. Wienholtz [1,‖]

[1] *Universität Greifswald, Institut für Physik, 17489 Greifswald, Germany*
[2] *Max-Planck-Institut für Kernphysik, Saupfercheckweg 1, 69117 Heidelberg, Germany*
[3] *Cyclotron Institute and Department of Physics, Texas A&M University, College Station, Texas 77843-4242, USA*
[4] *GSI Helmholtzzentrum für Schwerionenforschung GmbH, Planckstraße 1, 64291 Darmstadt, Germany*
[5] *Institut für Kernphysik, Universität zu Köln, Zülpicher Str. 77, D-50937 Köln, Germany*
[6] *Université Paris-Saclay, IN2P3/CNRS, IJCLab, 91405 Orsay, France*
[7] *CERN, 1211 Geneva, Switzerland*
[8] *University of Jyväskylä, Accelerator laboratory, 40014 Jyväskylä, Finland*
[9] *Helsinki Institute of Physics, FI-00014 Helsinki, Finland*

(Received 3 January 2026; accepted 18 February 2026; published 23 March 2026)

We report a high-precision mass measurement of ^{61}Zn, performed with the ISOLTRAP mass spectrometer at ISOLDE, CERN. Our result agrees with a recent measurement from the LEBIT Penning trap at FRIB and reduces the mass uncertainty by a factor of four. Combined with recent measurements of the mirror nuclide ^{61}Ga performed by TITAN at TRIUMF and CSRe at HIRFL, we obtain a more accurate Q value. This new value slightly improves the determination of the corresponding $\mathcal{F}t$ value in the $T_z = 1/2$ mirror beta decays used to test the conserved vector current hypothesis in the standard model.

DOI: 10.1103/fbf3-nry6

I. INTRODUCTION

Beta-decaying isotopes provide important tests for weak-interaction studies, which offer tantalizing possibilities for the discovery of new physics. The special class of Fermi beta transitions, in which the decaying nucleon spin is unchanged ($\Delta S = 0$) and the total nuclear momentum is conserved ($\Delta J = 0$), has provided the most stringent tests of the conserved vector current (CVC) hypothesis, concerning the independence of the weak interaction inside the nuclear medium. Fermi decays are also the basis of the V_{ud} element, decisive for testing the standard-model unitarity condition of the Cabbibo-Kobayashi-Maskawa (CKM) quark-mixing matrix in the standard model. The nuclear data required for such tests, including the decay energy, which is derived from mass measurements of the parent and daughter nuclides, has been periodically evaluated by Hardy and Towner, most recently in 2020 [1].

By extending this type of evaluation to the beta-decay transitions between $T = 1/2$ isospin doublets in mirror nuclei, Naviliat-Cuncic and Severijns have provided a complementary route to extract V_{ud} [2]. An essential step in these V_{ud} determinations is the calculation of the corrected $\mathcal{F}t \propto V_{ud}^{-2}$ value. This $\mathcal{F}t$ value is calculated from the product ft of statistical-rate function f and partial half-life t by including additional correction terms [3]. The statistical-rate function

$$f = \int_1^{W_0} pW(W_0 - W)^2 F(Z,W) C(Z,W)\, dW \qquad (1)$$

is an integral over the beta-decay energy spectrum, where $W = E_{\mathrm{kin}}/m_e c^2 + 1$ is the total beta energy, $p = \sqrt{W^2 - 1}$ is the beta momentum, and $W_0 = Q/m_e c^2 + 1$ the maximum beta energy. As this maximum energy is defined by the decay Q value, the Q value is the crucial experimental input to calculate f. $F(Z,W)$ is the Fermi function and $C(Z,W)$ includes a shape factor and higher-order corrections. The partial half-life

$$t = \frac{t_{1/2}}{\mathrm{BR}}(1 + P_{\mathrm{EC}}) \qquad (2)$$

consists of the electron-capture fraction P_{EC} and the two experimental inputs half-life $t_{1/2}$ and decay branching ratio BR. The input decay data have been measured with ever-improving precision. This fact, combined with advances in theoretical correction factors, has recently resulted in a more broad-ranging evaluation [3] that includes the weak

*Contact author: paul.giesel@uni-greifswald.de
†Present address: Belgian Nuclear Research Centre SCK CEN, Boeretang 200, 2400 Mol, Belgium.
‡Contact author: david.lunney@cnrs.fr
§Present address: CNRS International Research Laboratory for Nuclear Physics, Nuclear Astrophysics and Accelerator Technologies, TRIUMF, Vancouver, British Columbia, Canada.
‖Present address: Institut für Kernphysik, Technische Universität Darmstadt, 64289 Darmstadt, Germany.

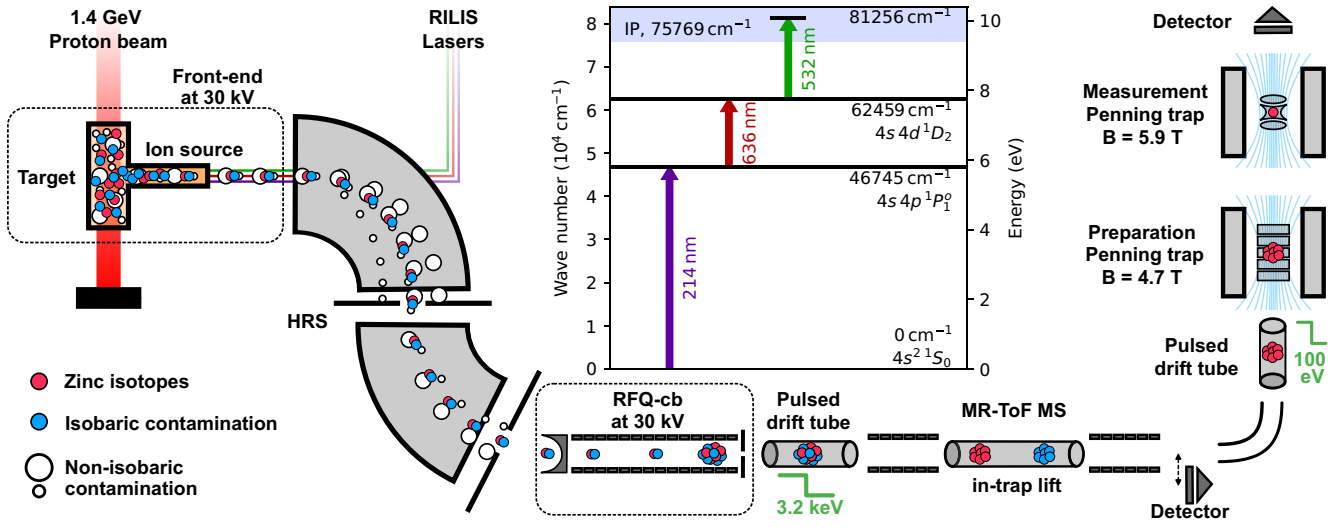

FIG. 1. Schematic representation of ISOLDE and the ISOLTRAP on-line mass spectrometer. The typical kinetic energy of the ions at various stages of the ISOLTRAP apparatus is indicated in green (for details, see Refs. [4,5]). The inset shows the RILIS laser-wavelength scheme employed to ionize Zn atoms from the target.

magnetism term, which is also of interest for testing the standard model through beta-decay correlation or spectrum-shape measurements. This most recent survey includes transitions and corrections up to—and including—the ^{61}Ga - ^{61}Zn mirror pair.

Although such decays require additional measurements to determine the respective Fermi (vector) and Gamow-Teller (axial-vector) components, the results achieve precision similar to constraints on V_{ud} coming from neutron decay.

In this work, we present a refined mass value for ^{61}Zn, obtained from complementary trapped-ion mass-spectrometry techniques. Thus, we update the input decay Q value by combining mass measurements of ^{61}Ga performed by the TITAN MR-ToF MS at TRIUMF [6] and Cooler Storage Ring (CSRe) at HIRFL, in Lanzhou [7]. The new Q value is, in turn, used to update the evaluation for beta-decay $\mathcal{F}t$ values presented in Ref. [3].

II. EXPERIMENT

The present measurements were performed at the radioactive ion-beam facility ISOLDE at CERN [8]. The ^{61}Zn^{+} ions of interest were produced by impinging a primary beam of 1.4-GeV protons from CERN's PS Booster accelerator on a Y_2O_3 target, shown schematically on the top left in Fig. 1. The zinc atoms diffusing out of the 1750-K heated target were ionized by multistep-resonance photoionization (RILIS) [9] according to the laser ionization scheme shown in the inset of Fig. 1. The zinc ions were accelerated to a kinetic energy of 30 keV, and the isobars of interest were mass-over-charge-ratio (m/q) selected using the ISOLDE High-Resolution (magnetic-dipole) Separator (HRS), depicted as the cut circles downstream of the ion source in Fig. 1.

The ISOLTRAP mass spectrometer [4,5] is schematically represented on the right-hand side of Fig. 1. The quasicontinuous ion beam from the HRS was transported to the ISOLTRAP spectrometer, where the ions were accumulated in a linear radio-frequency quadrupole cooler buncher (RFQ-cb) [10]. The RFQ-cb was floated to less than 100 eV below the 30 keV ion energy and filled with helium buffer gas. Collisions with the buffer gas stopped the ions in the trap and reduced their emittance. The ions were extracted in short bunches after 15 ms of cooling and bunching time, decelerated by a pulsed drift tube to a kinetic energy of 3.2 keV, and injected into a multi-reflection time-of-flight mass separator (MR-ToF MS) [11,12].

Enabled by its mass-resolving power in excess of 10^5, the MR-ToF MS was used as a mass filter to select the species of interest by optimizing the timing of its extraction pulse [13] to only extract the ion species of interest towards the Penning traps. The beam of selected ions was bent 90 degrees to ISOLTRAP's vertical section and captured in the preparation Penning trap [14], where the ions were further purified with the mass-selective buffer-gas cooling technique [15].

Finally, the mass-over-charge m_{ion}/q of the ion of interest was determined in the hyperbolic-measurement Penning trap by measuring the ion's cyclotron frequency

$$\nu_{\mathrm{c}} = \frac{qB}{2\pi m_{\mathrm{ion}}}, \tag{3}$$

via both the time-of-flight ion-cyclotron resonance (ToF-ICR) [16], and phase-imaging ion-cyclotron resonance (PI-ICR) [17] mass-spectrometry techniques. The magnetic field B was calibrated by measuring the cyclotron frequency $\nu_{\mathrm{c,ref}}$ of a reference species with a well-known mass $m_{\mathrm{ion,ref}}$ shortly before and shortly after the measurement of the species of interest. The measured cyclotron-frequency ratio

$$R = \frac{\nu_{\mathrm{c,ref}}}{\nu_{\mathrm{c}}} = \frac{m_{\mathrm{ion}}\, q_{\mathrm{ref}}}{m_{\mathrm{ion,ref}}\, q} \tag{4}$$

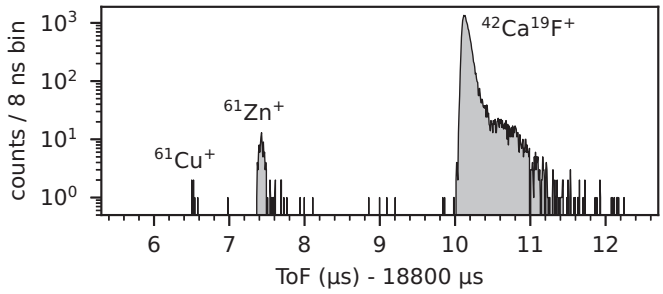

FIG. 2. Time-of-flight spectrum for ion identification recorded after 1000 revolutions in the MR-ToF MS. The abundant, stable ^{42}Ca^{19}F$^+$ contaminant was used as reference for the mass measurements of ^{61}Zn.

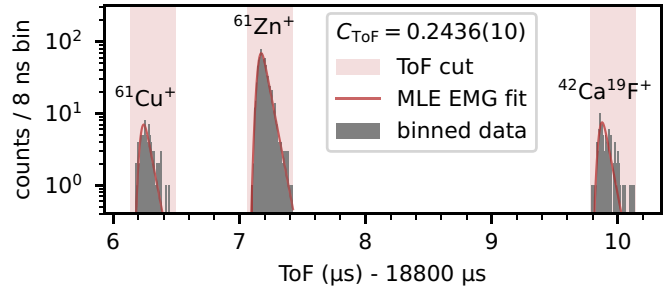

FIG. 3. Data used for the simultaneous unbinned maximum-likelihood estimation of C_{ToF} with the resulting EMG fit curves of the three ion species. The spectrum was recorded after 1000 revolutions in the MR-ToF MS.

was used to calculate the ion mass. In this work, all ions were singly charged. As the relevant electron and molecular binding energies are on the order of only a few electronvolts, far below the keV uncertainties of the measurements, they could be neglected in the calculation of mass if the neutral atom

$$m_{\text{atom}} = R\,(m_{\text{atom,ref}} - m_e) + m_e, \tag{5}$$

where m_e is the electron mass.

A. MR-ToF MS measurement

Multiple MR-ToF spectra were recorded using a MagneTOF detector [18] (bottom right in Fig. 1) during the identification of ion species in the beam and optimization of the experiment cycle, especially for choosing the proper timings for mass selective ejection out of the MR-ToF device [13]. An example of such a spectrum is shown in Fig. 2. The ^{61}Zn$^+$ ions were identified by observing their disappearance in the MR-ToF spectrum when turning off the element-specific resonant laser ionization, in addition to appearing at the expected ToF relative to the ^{42}Ca^{19}F$^+$ reference. Although intended only as a preparatory step, the MR-ToF spectra were later found to be suitable for an independent ^{61}Zn mass determination.

The fundamental relationship of time-of-flight (ToF) mass spectrometry,

$$t = a\sqrt{\frac{m_{\text{ion}}}{q}} + b, \tag{6}$$

links an ion's mass-over-charge ratio $\frac{m_{\text{ion}}}{q}$ to its flight time t [19]. In Eq. (6), a and b are parameters that are calibrated by measuring the flight times $t_{1,2}$ of two reference ions with well-known masses $m_{\text{ion},1}$ and $m_{\text{ion},2}$ and charges $q_{1,2}$. Here, ^{61}Cu$^+$ and ^{42}Ca^{19}F$^+$ were used as reference ions. The mass of an ion of interest is calculated from [20]

$$\sqrt{\frac{m_{\text{ion}}}{q}} = C_{\text{ToF}}\left(\sqrt{\frac{m_{\text{ion},1}}{q_1}} - \sqrt{\frac{m_{\text{ion},2}}{q_2}}\right) + \frac{1}{2}\left(\sqrt{\frac{m_{\text{ion},1}}{q_1}} + \sqrt{\frac{m_{\text{ion},2}}{q_2}}\right), \tag{7}$$

with the experimental value of

$$C_{\text{ToF}} = \frac{2t - t_1 - t_2}{2(t_1 - t_2)}. \tag{8}$$

For the present spectra, the ToF distribution of an ion species is well described by an exponentially modified Gaussian

$$EMG(t, \mu, \sigma, \tau) = \frac{1}{2\tau}\exp\left(\frac{\sigma^2}{2\tau^2} - \frac{t-\mu}{\tau}\right) \times \operatorname{erfc}\left(\frac{\sigma}{\sqrt{2}\tau} - \frac{t-\mu}{\sqrt{2}\sigma}\right),$$

where t is the time of flight, τ is the time constant of the exponential term, and σ^2 and μ are the variance and mean of the Gaussian term, respectively. For a specific experimental distribution $\vec{t}$ of flight times t_i of a single-ion species the unbinned negative log likelihood is

$$\ell(\vec{t}, \mu, \sigma, \tau) = -\sum_i \ln EMG(t_i, \mu, \sigma, \tau). \tag{9}$$

To obtain C_{ToF}, the ToF-distribution parameters of all three ion species are fitted simultaneously by minimizing

$$\ell(\vec{t}_{\text{Cu}}, \mu_{\text{Cu}}, \sigma, \tau) + \ell\left(\vec{t}_{\text{Zn}}, \mu_{\text{Zn}} = C_{\text{ToF}}(\mu_{\text{Cu}} - \mu_{\text{CaF}}) + \frac{\mu_{\text{Cu}} + \mu_{\text{CaF}}}{2}, \sigma, \tau\right) + \ell(\vec{t}_{\text{CaF}}, \mu_{\text{CaF}}, \sigma, \tau).$$

To reduce systematic effects such as detector saturation, for each species' ToF window, only cycles containing a single-ion

TABLE I. Final frequency ratios (R), time-of-flight ratio (C_{ToF}), and mass excess (ME) of the ^{61}Zn$^+$ measured in this work.

Method	Reference Ions	Ratio R or C_{ToF}	ME (keV)
MR-ToF	^{61}Cu$^+$, ^{42}Ca^{19}F$^+$	0.2436(10)	−56 356(22)
ToF-ICR	^{42}Ca^{19}F$^+$	0.999 712 527(59)	−56 357.6 (33)
	^{85}Rb$^+$	0.717 678 235(36)	−56 357.0 (29)
PI-ICR	^{42}Ca^{19}F$^+$	0.999 712 574(24)	−56 355.0 (14)
	Weighted average		−56 355.4 (13)

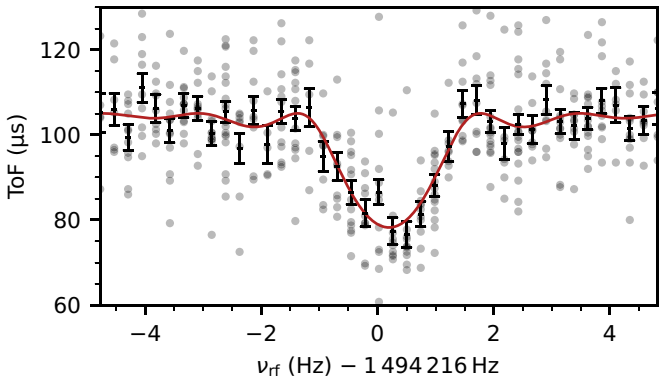

FIG. 4. A typical ToF-ICR resonance of $^{61}Zn^{+}$, with a 600 ms excitation time. The grey points represent the flight times of the individual ions recorded after ejection at different excitation frequencies ν_{rf}. The black errorbars represent the mean ToF at each frequency step while the red line shows the result of the least-squares fit of these mean values to the theoretical line shape [21].

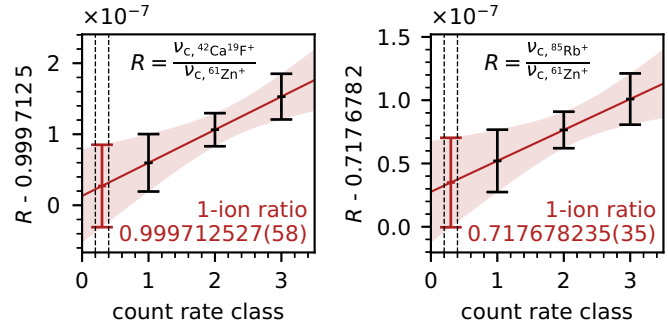

FIG. 6. Single-ion extrapolation of the ToF-ICR frequency ratio R for $^{61}Zn^{+}$ with $^{42}Ca^{19}F^{+}$ and $^{85}Rb^{+}$ references. The black error bars show the results for the three count-rate classes while the red line shows the extrapolated linear dependence with the corresponding error band in light red. The extrapolated R for a single ion in the trap is indicated by the red error bar. The detector efficiency of 0.3(1) is marked by the dashed vertical lines.

count in the window were included. Note that this excludes a large number of $^{42}Ca^{19}F^{+}$ counts and their relative intensity is therefore lower than in Fig. 2. The three ion arrival-time signals ($\vec{t}_{Cu}$, $\vec{t}_{Zn}$, and $\vec{t}_{CaF}$) and the associated fitted EMGs are shown in Fig. 3 while the resulting C_{ToF} and the derived-mass excess are listed in Table I together with the ICR-MS results.

B. ToF-ICR measurement

For the ToF-ICR measurement in the precision Penning trap, a 3-ms-long dipole excitation at the ions' magnetron frequency increased the ions' magnetron radius. Next, a quadrupolar excitation at the cyclotron frequency converted the ions' magnetron motion into cyclotron motion. As the latter has a much higher frequency, the ions' magnetic moment increased. Finally, the ions were ejected out of the Penning trap onto the detector where their ToF was measured. When the ions leave the trap axially along the magnetic-field direction, their orbital magnetic moment leads to a conversion of their transversal kinetic energy into longitudinal kinetic

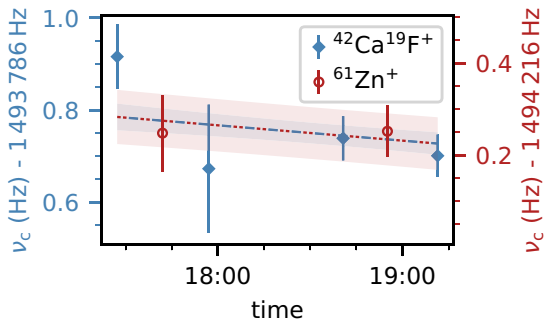

FIG. 5. Simultaneous least-squares fit of a first-degree polynomial to the zinc and the calcium-fluoride ToF-ICR frequencies to obtain the frequency ratio R. This example shows the data for one detected count per measurement cycle.

energy, thereby reducing the ions' ToF. This measurement cycle was repeated for different excitation frequencies ν_{rf}, where the lowest flight time was achieved when this frequency matched the ions' cyclotron frequency ν_c.

An example of such a ToF-ICR scan for $^{61}Zn^{+}$ is shown in Fig. 4, where the theoretical line shape [21] is fitted to the data to obtain the cyclotron frequency. The quadrupolar-excitation time for $^{61}Zn^{+}$ was 600 ms, while 1200 ms was used for the stable $^{42}Ca^{19}F^{+}$ and $^{85}Rb^{+}$ reference ions. According to Eq. (4), only one reference is required to obtain the mass of the ion of interest. A second reference species was taken for a cross check.

The frequency ratios R between zinc and reference ions were determined with a simultaneous polynomial fit of their frequencies over time, similar to Ref. [22], see Fig. 5. To also account for a systematic effect of different number of ions in the trap, the data was divided into three groups with 1, 2, and 3 ions measured per ejection cycle. In a least-squares minimization, the same polynomial was fitted simultaneously to the zinc and the reference data for all three count-rate classes, with each polynomial multiplied only by a scaling factor. The frequency ratio R was determined from the ratio of the zinc and reference-ion scaling factors. For each ion species, the scaling factors of the three count-rate classes were fixed to a linear trend. This linear fit allowed the extrapolation to the single-ion frequency ratio [23] using a calculated detector efficiency of 0.3(1), as shown in Fig. 6.

The ISOLTRAP mass-dependent systematic effect and residual uncertainty from Ref. [23] are included in the uncertainty of the ToF-ICR frequency ratio R and the derived-mass excess listed in Table I.

C. PI-ICR measurement

The measurement scheme employed for the PI-ICR measurement of ν_c is extensively described in Ref. [24] (denoted as scheme 2). In short, three separate ion-position measurements are made. First, the center of the ions' radial motion is determined by ejecting the ions with minimized radial-motion

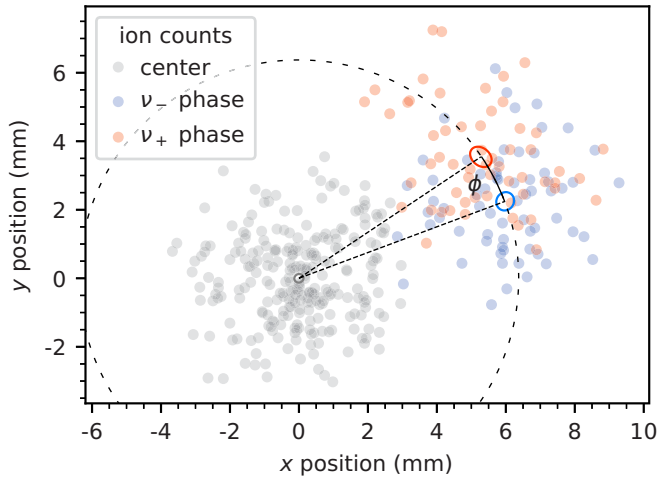

FIG. 7. Example of PI-ICR spots of $^{61}Zn^+$ recorded on a position-sensitive microchannel-plate particle detector. The full circles represent ion counts. The corresponding unfilled ellipses represent the 1σ-uncertainty band of the fitted spot position using a multivariate Gaussian distribution [22]. In this example, the ions in magnetron and cyclotron orbits accumulated a total of $n_- + n_+ =$ 720 000 revolutions ($t_{acc} \approx 0.48$ s phase-accumulation time). The resulting phase difference ϕ is indicated.

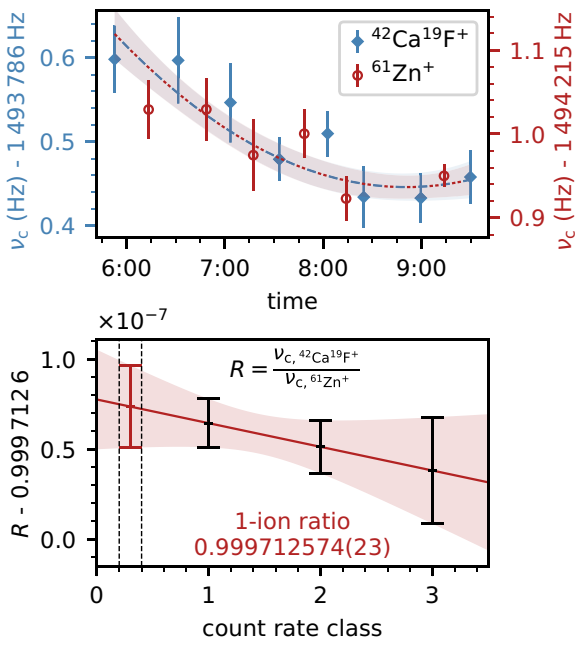

FIG. 8. Top: Simultaneous least-squares fit of a second-degree polynomial to the zinc and reference PI-ICR frequencies to obtain the frequency ratio R. This example shows the data for one detected count per measurement cycle. Bottom: Single-ion extrapolation of R. The black error bars show the R results for the three count-rate classes while the red line shows the extrapolated linear dependence with the corresponding error band in light red. The extrapolated R with a single ion in the trap is indicated by the red error bar. The detector efficiency of 0.3(1) is marked by the dashed vertical lines.

amplitudes. In both the second and third measurements, the ions are initially put on a cyclotron orbit with minimized magnetron motion by a dipole pulse at ν_- followed by a dipole excitation at ν_+. In the second measurement, the resulting cyclotron motion at the reduced-ion cyclotron frequency ν_+ is immediately converted into a magnetron motion by a quadrupolar π pulse at ν_c. Subsequently, the ion orbits in the trap for a phase-accumulation time t_{acc} before being ejected to the detector. When the ion leaves the magnetic field of the trap, its magnetron radius is magnified, allowing for precise measurement of the ions' magnetron phase ϕ_- from their position on the detector. Finally to measure ϕ_+, in the third measurement the ions revolve on the cyclotron orbit for t_{acc} before being converted by the π pulse at ν_c to achieve the same magnification as in the second measurement. An example of the resulting three ion spots is shown in Fig. 7. By knowing the number of revolutions n_- and n_+ the ions performed in measurements two and three, one can use the angle ϕ between the two recorded ion spots to calculate the ions' cyclotron frequency [23]

$$\nu_c = \nu_- + \nu_+ = \frac{2\pi(n_- + n_+) + \phi}{2\pi t_{acc}}. \tag{10}$$

The fit procedure to obtain ϕ for each measurement is described in detail in Ref. [22]. Similarly to the ToF-ICR measurement, the frequency of $^{61}Zn^+$ and the $^{42}Ca^{19}F^+$ reference are recorded alternately, allowing a simultaneous polynomial fit to obtain their frequency ratio (see top plot of Fig. 8). Again, the data is divided into count-rate classes for the extrapolation of the single-ion ratio as shown on the bottom plot of Fig. 8. Conservatively, the same residual uncertainty [24] as in the ToF-ICR measurement is added in quadrature to the frequency ratio R uncertainty listed in Table I.

III. DISCUSSION

The mass-excess results from the three different methods of trapped-ion mass spectrometry are listed in Table I. While the result derived from the MR-ToF measurement has an uncertainty almost one order of magnitude larger than the others, its value is in perfect agreement. In Fig. 9, we compare the MR-ToF, ToF-ICR, and PI-ICR results, along with the ToF-ICR result from LEBIT [25], all of which agree within one standard deviation. The result of this work reduces the uncertainty of the ^{61}Zn mass value by a factor of four, thereby dominating the weighted average of all previous measurements.

The decay Q value is the mass difference of mother and daughter nuclide. As evident from Eq. (1), the $\mathcal{F}t$ value of the ^{61}Ga - ^{61}Zn mirror decay depends sensitively on this Q value. The last $\mathcal{F}t$ survey by Severijns *et al.* [3] used the AME 2020 Q value for this decay [26]. Since then, in addition to the more precise mass of ^{61}Zn presented here, two measurements of ^{61}Ga have been published: a TITAN-MRTOF measurement by Paul *et al.* [6], yielding −47114(12) keV, and an isochronous-mode storage-ring measurement by Wang *et al.* [7], with a result of −47168(21) keV. While these two recent values differ by almost two standard deviations, the

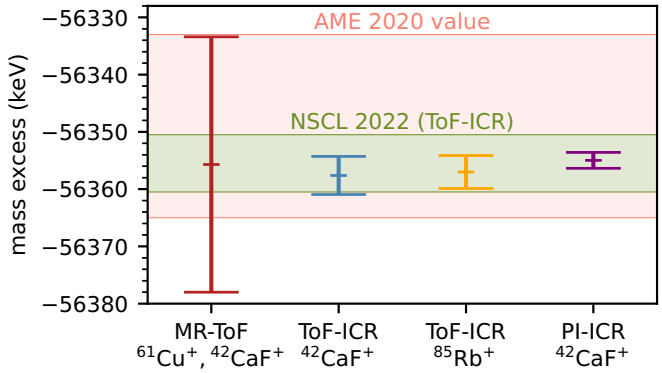

FIG. 9. The present ^{61}Zn results compared to the AME2020 [26] and recent NSCL result [25]. The references used for the different measurements are indicated below the methods in the labels on the abscissa.

least-squares weighted average of them and the older AME value is −47127(10) keV.[1] This yields a new decay Q value of: 9228(10) keV, compared to the AME2020 value of 9214(38) keV used by Severijns *et al.* [3,26].

Awaiting an updated mirror-transition evaluation, we have used the "LogFT calculator" provided by NNDC [28] to calculate $\log_{10}(\mathcal{F}t)$. In addition to the decay Q value, the calculator requires a transition intensity and decay half-life, which we have taken from Ref. [3]. The result is $\log_{10}(\mathcal{F}t) = 3.681(9)$, which compares to $\log_{10}(\mathcal{F}t) = 3.677(13)$ obtained in Ref. [3]. The new value has a slightly reduced uncertainty but the two results agree well within their uncertainties. The nucleus-dependent correction terms (described in Ref. [3]) to convert the ft value into an $\mathcal{F}t$ value for comparison with other mirror transitions may also be improved in the future.

Figure 3 in Ref. [3] shows the fractional contribution of the experimental and theoretical input factors to the $\mathcal{F}t$ values for the mirror beta transitions in the mass range $A = 41$–61. The Q value for the $A = 61$ case contributes the largest uncertainty to all the cases shown in the figure, at 2.2%. For the present work, Fig. 10 shows the experimental uncertainties of the ^{61}Ga - ^{61}Zn decay with the values used by Ref. [3] in gray and the new Q value in yellow. Our result helps to bring this uncertainty contribution below that of the decay half-life and branching-ratio inputs. This motivates future, more precise measurements of those two values. Additionally, the two-standard-deviation discrepancy in the ^{61}Ga mass excesses provides a strong motivation for a Penning-trap mass measurement, which could reduce the uncertainty by an order of magnitude.

[1]When taking the weighted standard deviation [27] instead of the standard error of the weighted mean, the combined uncertainty would be 28 keV. This would result in $\log_{10}(\mathcal{F}t) = 3.681(11)$.

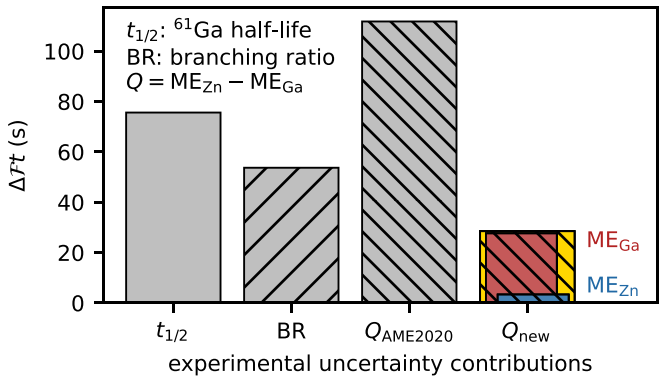

FIG. 10. Uncertainty contributions of the experimental input factors to the $\mathcal{F}t$ value for the ^{61}Ga - ^{61}Zn mirror beta transition. The gray uncertainty contributions are the same as in Ref. [3] and the new Q value is indicated in yellow with the partial contribution from the ^{61}Ga mass excess in red and the ^{61}Zn mass excess from this work in blue.

IV. CONCLUSION

The mass of ^{61}Zn was measured with the ISOLTRAP mass spectrometer at ISOLDE using multiple state-of-the-art techniques. The uncertainty of the ^{61}Zn mass value was reduced by a factor of four. This result helped to lower the uncertainty of the Q value of the mirror beta decay, which in turn, reduces the Q-value uncertainty contribution for the determination of the $\mathcal{F}t$ value. Consequently, it provides a strong incentive for more precise measurements of the decay half-life and branching ratio. A detailed re-evaluation of the latest data for these types of decays will show their impact on the conserved vector current (CVC) hypothesis and determination of V_{ud} to probe for physics beyond the standard model.

ACKNOWLEDGMENTS

We thank the ISOLDE technical group and the ISOLDE Collaboration for their support. We acknowledge support from the Max Planck Society, the German Federal Ministry of Education and Research (BMBF) (Contracts No. 05P15HGCIA, No. 05P18HGCIA, and No. 05P21HGCI1), the Institut National de Physique Nucléaire et de Physique des Particules (IN2P3), and the European Union's Horizon 2020 research and innovation programme (Grants No. 654002 and No. 771036).

The experiment was conducted by L.N., M.M., V.A.V., P.F., D.A., F.W., I.K., Yu.A.L., and D.L. Resources and supervision were provided by K.B., D.L., and L.S. Data analysis was performed by P.F.G. and J.K. The manuscript was prepared by P.F.G. and D.L. Additionally, D.A., K.B., J.K., Yu.A.L., L.N., L.S., and V.A.V. have contributed to the editing of the manuscript.

DATA AVAILABILITY

The data that support the findings of this article are openly available [29].

[1] J. C. Hardy and I. S. Towner, Superallowed $0^+ \to 0^+$ nuclear β decays: 2020 critical survey, with implications for V_{ud} and CKM unitarity, Phys. Rev. C **102**, 045501 (2020).

[2] O. Naviliat-Cuncic and N. Severijns, Test of the conserved vector current hypothesis in $T = 1/2$ mirror transitions and new determination of $|V_{ud}|$, Phys. Rev. Lett. **102**, 142302 (2009).

[3] N. Severijns, L. Hayen, V. De Leebeeck, S. Vanlangendonck, K. Bodek, D. Rozpedzik, and I. S. Towner, $\mathcal{F}t$ values of the mirror β transitions and the weak-magnetism-induced current in allowed nuclear β decay, Phys. Rev. C **107**, 015502 (2023).

[4] M. Mukherjee, D. Beck, K. Blaum, G. Bollen, J. Dilling, S. George, F. Herfurth, A. Herlert, A. Kellerbauer, H. J. Kluge, S. Schwarz, L. Schweikhard, and C. Yazidjian, ISOLTRAP: An on-line Penning trap for mass spectrometry on short-lived nuclides, Eur. Phys. J. A **35**, 1 (2008).

[5] S. Kreim, *et al.*, Recent exploits of the ISOLTRAP mass spectrometer, Nucl. Instrum. Meth. B **317**, 492 (2013).

[6] S. F. Paul, *et al.*, Mass measurements of $^{60-63}$Ga reduce x-ray burst model uncertainties and extend the evaluated $T = 1$ isobaric multiplet mass equation, Phys. Rev. C **104**, 065803 (2021).

[7] M. Wang, *et al.*, Mass measurement of upper fp-shell $N = Z - 2$ and $N = Z - 1$ nuclei and the importance of three-nucleon force along the $N = Z$ line, Phys. Rev. Lett. **130**, 192501 (2023).

[8] R. Catherall, *et al.*, The ISOLDE facility, J. Phys. G: Nucl. Part. Phys. **44**, 094002 (2017).

[9] V. Fedosseev, K. Chrysalidis, T. D. Goodacre, B. Marsh, S. Rothe, C. Seiffert, and K. Wendt, Ion beam production and study of radioactive isotopes with the laser ion source at ISOLDE, J. Phys. G: Nucl. Part. Phys. **44**, 084006 (2017).

[10] F. Herfurth, J. Dilling, A. Kellerbauer, G. Bollen, S. Henry, H.-J. Kluge, E. Lamour, D. Lunney, R. Moore, C. Scheidenberger, S. Schwarz, G. Sikler, and J. Szerypo, A linear radiofrequency ion trap for accumulation, bunching, and emittance improvement of radioactive ion beams, Nucl. Instrum. Meth. A **469**, 254 (2001).

[11] R. Wolf, *et al.*, On-line separation of short-lived nuclei by a multi-reflection time-of-flight device, Nucl. Instrum. Meth. A **686**, 82 (2012).

[12] R. Wolf, F. Wienholtz, *et al.*, ISOLTRAP's multi-reflection time-of-flight mass separator/spectrometer, Int. J. Mass Spectrom. **349–350**, 123 (2013).

[13] F. Wienholtz, S. Kreim, M. Rosenbusch, L. Schweikhard, and R. Wolf, Mass-selective ion ejection from multi-reflection time-of-flight devices via a pulsed in-trap lift, Int. J. Mass Spectrom. **421**, 285 (2017).

[14] H. Raimbault-Hartmann, D. Beck, G. Bollen, M. König, H.-J. Kluge, E. Schark, J. Stein, S. Schwarz, and J. Szerypo, A cylindrical Penning trap for capture, mass selective cooling, and bunching of radioactive ion beams, Nucl. Instrum. Meth. B **126**, 378 (1997).

[15] G. Savard, S. Becker, G. Bollen, H.-J. Kluge, R. Moore, T. Otto, L. Schweikhard, H. Stolzenberg, and U. Wiess, A new cooling technique for heavy ions in a Penning trap, Phys. Lett. A **158**, 247 (1991).

[16] F. G. Kondev, M. Wang, W. J. Huang, S. Naimi, and G. Audi, The NUBASE2020 evaluation of nuclear physics properties, Chinese Phys. C **45**, 030001 (2021).

[17] S. Eliseev, K. Blaum, M. Block, C. Droese, M. Goncharov, E. Minaya Ramirez, D. A. Nesterenko, Y. N. Novikov, and L. Schweikhard, Phase-imaging ion-cyclotron-resonance measurements for short-lived nuclides, Phys. Rev. Lett. **110**, 082501 (2013).

[18] D. Stresau, K. Hunter, W. Sheils, P. Raffin, and Y. Benari, A new class of robust sub-nanosecond TOF detectors with high dynamic range (2006), https://www.etp-ms.com/file-repository/26.

[19] M. Guilhaus, Special feature: Tutorial. Principles and instrumentation in time-of-flight mass spectrometry. Physical and instrumental concepts, J. Mass Spectrom. **30**, 1519 (1995).

[20] F. Wienholtz, *et al.*, Masses of exotic calcium isotopes pin down nuclear forces, Nature (London) **498**, 346 (2013).

[21] M. König, G. Bollen, H.-J. Kluge, T. Otto, and J. Szerypo, Quadrupole excitation of stored ion motion at the true cyclotron frequency, Int. J. Mass Spectrom. **142**, 95 (1995).

[22] J. Karthein, D. Atanasov, K. Blaum, D. Lunney, V. Manea, and M. Mougeot, Analysis methods and code for very high-precision mass measurements of unstable isotopes, Comput. Phys. Commun. **267**, 108070 (2021).

[23] S. Eliseev, *et al.*, A phase-imaging technique for cyclotron-frequency measurements, Appl. Phys. B **114**, 107 (2014).

[24] A. Kellerbauer, K. Blaum, G. Bollen, F. Herfurth, H.-J. Kluge, M. Kuckein, E. Sauvan, C. Scheidenberger, and L. Schweikhard, From direct to absolute mass measurements: A study of the accuracy of ISOLTRAP, Eur. Phys. J. D **22**, 53 (2003).

[25] Z. Meisel, A. Hamaker, *et al.*, Improved nuclear physics near $A = 61$ refines urca neutrino luminosities in accreted neutron star crusts, Phys. Rev. C **105**, 025804 (2022).

[26] M. Wang, W. Huang, F. Kondev, G. Audi, and S. Naimi, The AME 2020 atomic mass evaluation (II). Tables, graphs and references, Chinese Phys. C **45**, 030003 (2021).

[27] N. A. Heckert and J. J. Filliben, Weighted standard deviation, in *NIST Handbook 148: Dataplot Reference Manual* (NIST, 2003), Vol. 2, Chap. 2.

[28] LogFT tool of the National Nuclear Data Center, Brookhaven National Laboratory: https://www.nndc.bnl.gov/logft/ (2025).

[29] P. F. Giesel, *et al.*, Dataset: Precision mass measurement of 61Zn and updated *Ft* value for conserved vector current tests [Data set], Zenodo, (2026) https://doi.org/10.5281/zenodo.18939265.